Ion damage buildup and amorphization processes in GaAs–$Al_xGa_{1-x}As$ multilayers

H. H. Tan, C. Jagadish, J. S. Williams, J. Zou, and D. J. H. Cockayne

Citation: Journal of Applied Physics **80**, 2691 (1996); doi: 10.1063/1.363186

View online: https://doi.org/10.1063/1.363186

View Table of Contents: http://aip.scitation.org/toc/jap/80/5

Published by the American Institute of Physics

Ion damage buildup and amorphization processes in GaAs–$Al_xGa_{1-x}As$ multilayers

H. H. Tan,[a] C. Jagadish, and J. S. Williams
Department of Electronic Materials Engineering, Research School of Physical Sciences and Engineering, The Australian National University, Canberra 0200, Australia

J. Zou and D. J. H. Cockayne
Electron Microscope Unit, The University of Sydney, New South Wales 2006, Australia

(Received 2 October 1995; accepted for publication 20 May 1996)

The nature of ion damage buildup and amorphization in GaAs–$Al_xGa_{1-x}As$ multilayers at liquid-nitrogen temperature is investigated for a variety of compositions and structures using Rutherford backscattering-channeling and cross-sectional transmission electron microscopy techniques. In this multilayer system, damage accumulates preferentially in the GaAs layers; however, the presence of AlGaAs enhances the dynamic annealing process in adjacent GaAs regions and thus amorphization is retarded close to the GaAs–AlGaAs interfaces even when such regions suffer maximum collisional displacements. This dynamic annealing in AlGaAs and at GaAs–AlGaAs interfaces is more efficient with increasing Al content; however, the dynamic annealing process is not perfect and an amorphous phase may be formed at the interface above a critical defect level or ion dose. Once an amorphous phase is nucleated, amorphization proceeds rapidly into the adjacent AlGaAs. This is explained in terms of the interplay between defect migration and defect trapping at an amorphous–crystalline or GaAs–AlGaAs interface. In addition, enhanced recrystallization of the amorphous GaAs at the interface may occur during heating if an amorphous phase is not formed in the adjacent AlGaAs layer. This is most likely the result of mobile defects injected from the AlGaAs layer during heating.
[S0021-8979(96)00817-1]

INTRODUCTION

The electrical, optical, and band-gap properties of lattice-matched GaAs–AlGaAs heterostructures make them one of the most important material systems for optoelectronic devices. The discovery of impurity-induced layer disordering by Laidig *et al.*[1] has stimulated considerable interest in the study of disordering behavior and impurity-damage interactions in these multilayer structures. Since it was demonstrated that ion implantation can also induce the same disordering effect,[2] but in certain localized regions, nanofabrication of novel photonic devices, such as passive waveguides and quantum wires/dots, has been reported.[3–5] Irradiation-induced intermixing leads to a change in the local band gap and refractive index of the material, thus making it a useful processing tool for optical isolation and other photonic integrated circuit applications.[6–8] The use of ion implantation in creating highly resistive regions for electrical isolation of GaAs–AlGaAs heterojunction bipolar transistors (HBTs) has also recently been demonstrated.[9,10] As such, in order to optimize device performance by introducing a controllable amount of damage in multilayer structures, it is important to study the ion-beam-induced damaging processes in these multilayer structures.

Recent studies[11–22] have shown that in GaAs–AlAs or GaAs–AlGaAs heterostructures damage is preferentially formed in GaAs or AlGaAs layers with the lower Al composition. Also, resistance to amorphization in AlGaAs increases with Al content. The disordering process in these multilayer structures becomes significantly more complex due to the competing disordering and annealing processes at the interfaces. Several, somewhat conflicting, processes have been proposed to play dominant roles in damage accumulation in multilayers such as defect migration, atomic intermixing, and differences in the electronic stopping effects of the ions. Indeed, a thorough understanding of damage formation and annealing processes in GaAs–AlGaAs structures is lacking. In order to resolve some of the complexities in this multilayer material system, we have recently studied the damage buildup and amorphization processes in thick (bulk) AlGaAs samples of various Al compositions. Our results show that efficient dynamic annealing occurs during implantation at liquid-nitrogen temperatures and, as a result, damage accumulation in AlGaAs is significantly more complicated than in GaAs.[23] This effect is further complicated by the different mechanisms of damage formation in both GaAs and AlGaAs (AlAs). Using these results as a platform, we have specifically engineered the multilayer structures and ion-beam conditions in this study to specifically probe the details of ion damage buildup and amorphization processes in GaAs–AlGaAs multilayers. Damage induced by both keV and MeV Si ion-beam irradiation at liquid-nitrogen temperatures is systematically investigated using ion channeling and transmission electron microscopy techniques.

EXPERIMENT

All structures in this work were grown on epiready VGF semi-insulating GaAs (100) substrates using the low-pressure (76 Torr) metal-organic chemical-vapor-deposition

[a]Electronic mail: hoe109@rphysse.anu.edu.au

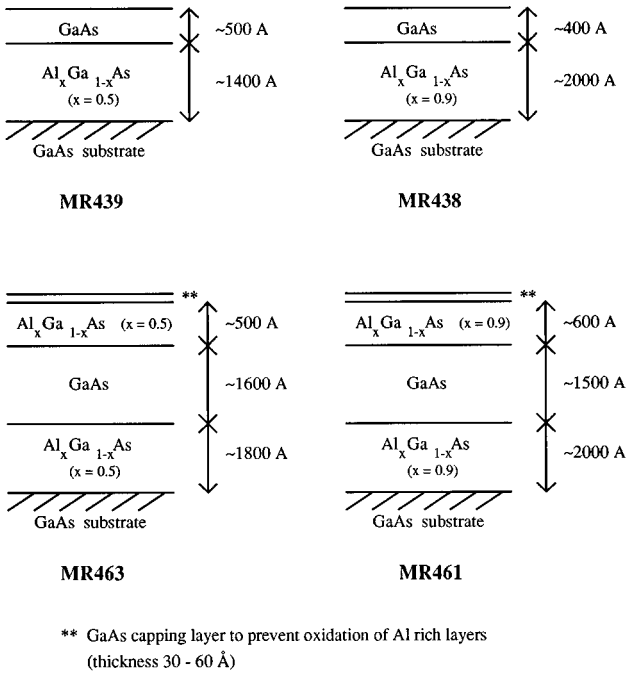

FIG. 1. Schematic of the various multilayer structures used in this study.

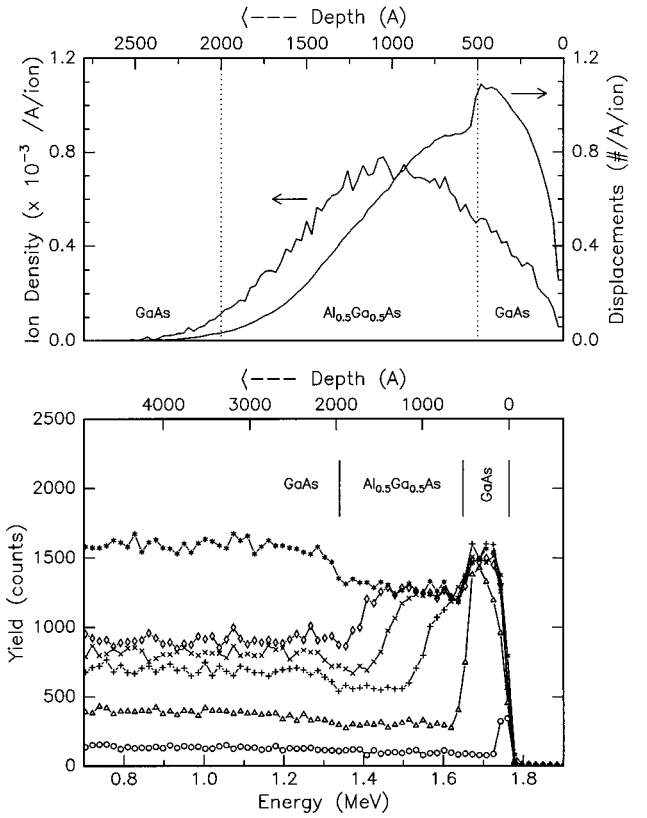

FIG. 2. RBS-C spectra (lower panel) showing the damage buildup for 90 keV Si^- irradiation of GaAs/$Al_{0.5}Ga_{0.5}As$/GaAs multilayer (MR439) at liquid-nitrogen temperature for various doses: unimplanted (○);6×10^{13} cm^{-2} (△); 1×10^{14} cm^{-2} (+); 2×10^{14} cm^{-2} (×); 5×10^{14} cm^{-2} (◇); and random spectrum (∗). Also shown in the upper panel is the displacement density profile as calculated by FASTRIM (Ref. 25).

reactor at the Australian National University (ANU). All growths were carried out at 750 °C with trimethylgallium (TMG) and trimethylaluminium (TMA) as the group-III sources and arsine as the group-V source. An initial GaAs buffer layer with a thickness of about 0.5–1 μm was first grown on all samples. Two sets of structures, each with two $Al_xGa_{1-x}As$ compositions were grown $x=0.5$ and 0.9). One set had an AlGaAs layer sandwiched between two GaAs layers and the other a GaAs layer in between two AlGaAs layers. The purpose here is to provide a direct comparison between the two cases. Figure 1 summarizes the various structures used in this study. Irradiation was carried out using the ANU 1.7 MV tandem accelerator with 90 keV Si^-, 1 MeV Si^+ or 4 MeV Si^+ ions. For the keV irradiation, the nuclear energy deposition varied significantly across the layers while MeV ions were used to obtain a fairly uniform nuclear energy deposition profile across the layers. During implantation, samples were held at liquid-nitrogen (LN2) temperature and tilted 7° away from the beam axis to minimize channeling effects. The ion dose was in the range of 6×10^3 to 3×10^{16} cm^{-2} and the dose rates were kept low enough to minimize any beam heating. Analysis was carried out at room temperature by using the Rutherford backscattering-channeling (RBS-C) technique with 2 MeV He^+ ions. A Si surface barrier detector was set at a scattering angle of 100° to improve depth resolution in the regions of interest. Selected samples were then analyzed by cross-sectional transmission electron microscopy (XTEM). Two methods were used to prepare XTEM samples. To see the basic structure of the (unimplanted) samples, a cleavage method was used in which the samples were cleaved along two orthogonal ⟨110⟩ directions on the (001) plane and after which the samples were observed through the right-angle edge. To study the microstructures and defects of the (implanted) samples, the specimens were prepared by ion beam thinning with a cold stage. All XTEM samples were studied using the Philips EM 430 microscope operating at 300 keV.

RESULTS

The RBS-C results for an $A1_{0.5}Ga_{0.5}As$ layer sandwiched between two GaAs layers (MR439) irradiated with 90 keV Si^- are shown in Fig. 2. Also shown in this figure are the displacement density and the ion range distribution of the ions as calculated by a modified version of TRIM85-90,[24] FASTRIM,[25] which corrects the interfacial problems inherent with TRIM. The displacement density rises steeply in the top GaAs layer, reaching a maximum at the interface and decreases across the AlGaAs layer. At the lower interface, the displacement density has dropped by about an order of magnitude compared with the top interface. The experimental results show that damage builds up preferentially in the top GaAs layer. At a dose of 6×10^{13} cm^{-2}, the top GaAs appears to be heavily damaged; however, complete amorphization has not yet resulted (note that the aligned spectrum has not quite reached the random level), and the damage profile corresponds well to the displacement distribution. The underlying $Al_{0.5}Ga_{0.5}As$ layer, on the other hand, remains crystalline with very little observable damage. This strong differ-

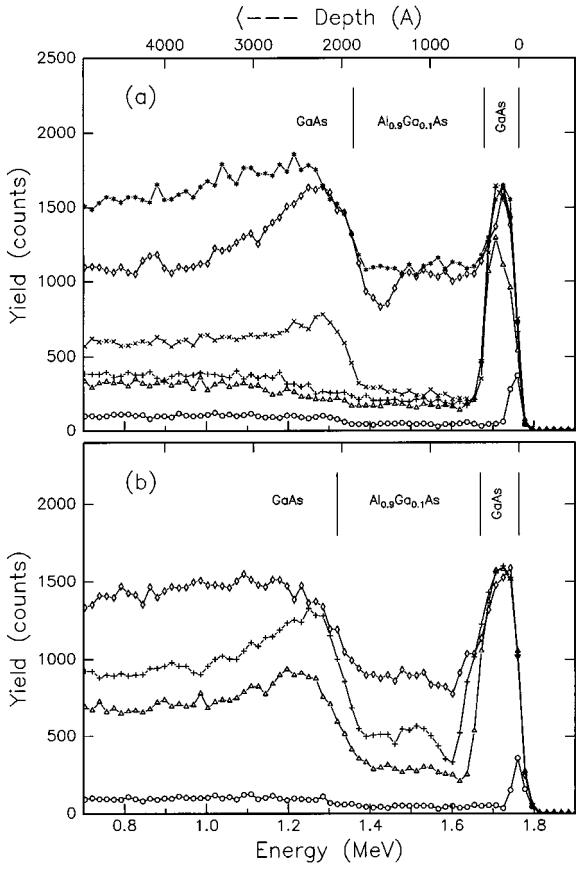

FIG. 3. RBS-C spectra showing the damage buildup for 90 keV Si^- irradiation of GaAs/$Al_{0.9}Ga_{0.9}As$/GaAs multilayer (MR438) at liquid-nitrogen temperature for various doses. Due to a slight layer thickness inhomogeneity across the wafer, two sets of spectra (at constant layer thickness) are shown: (a) for unimplanted (○), 6×10^{13} cm^{-2} (△), 1×10^{14} cm^{-2} (×), 1×10^{15} cm^{-2} (×), 1×10^{16} cm^{-2} (◇), and random spectrum (*); and (b) for unimplanted (○) 5×10^{15} cm^{-2} (△), 8×10^{15} cm^{-2} (+), and random spectrum (◇).

ential damage effect is quite interesting since the difference in the maximum displacements between the two materials is only about 25% but is consistent with the well-known observations that AlGaAs with increasing Al content is more resistant to ion-beam damage.[11–16,23] At a dose of $1\times10^{14}cm^{-2}$, amorphization of the GaAs overlayer occurs, extending rapidly across the interface into the $Al_{0.5}Ga_{0.5}As$ layer. With further increase in irradiation dose, the amorphous layer grows from the interface further into the $Al_{0.5}Ga_{0.5}As$ layer. No damage is observable at the bottom interface due to the low density of displacements. The interesting point to note here is that, once an amorphous phase is formed at the GaAs–$Al_{0.5}Ga_{0.5}As$ interface, amorphization of $Al_{0.5}Ga_{0.5}As$ proceeds very rapidly, suggesting that an amorphous–crystalline interface acts as a sink for defects which are mobile in AlGaAs and hence a preferential nucleating site for amorphization. This is discussed more fully later.

Figure 3(a) and 3(b) illustrate the RBS-C results of 90 keV Si^- irradiation of sample MR438, which is structurally similar to the one above but with a higher Al content ($Al_{0.9}Ga_{0.1}As$). The displacement density and the ion range

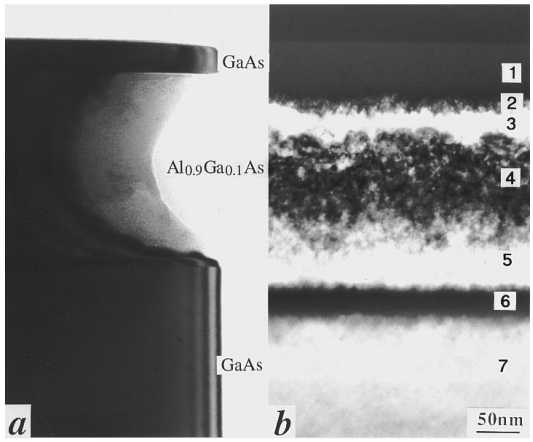

FIG. 4. (a) Bright-field XTEM image of a cleavage specimen from an unimplanted sample as in Fig. 3 (MR438) showing the basic structure, and (b) 400 dark-field XTEM image of the same sample implanted to a dose of 8×10^{15} cm^{-2}. Both images have identical magnification.

distribution are similar to that of Fig. 2 with about 30% difference in the maximum displacement density across the top interface. The projected range of ions R_p is at ~1100 Å, which lies well in the $Al_{0.9}Ga_{0.1}As$ layer. At a dose of 6×10^{13} cm^{-2}, the overlaying GaAs layer appears to be heavily defected while the underlying $Al_{0.9}Ga_{0.1}As$ layer remains almost defect free. Amorphization of the GaAs layer occurs at 1×10^{14} cm^{-2}; however, in this case the $Al_{0.9}Ga_{0.1}As$ layer is able to resist amorphization across the interface up to higher doses than for $Al_{0.5}Ga_{0.5}As$. In fact, at a dose of 1×10^{15} cm^{-2}, a buried damage peak is observable close to the deeper interface in the underlying GaAs layer (at ~2500 Å) but good crystallinity is still preserved in the $Al_{0.9}Ga_{0.1}As$ layer. Although this damage peak is located in the tail of the displaced atom distribution, the ion dose is sufficient for a significant damage accumulation in GaAs in this region. Eventually, a buried continuous amorphous layer is formed in the GaAs below the deep AlGaAs interface, with further increase in irradiation dose. Very little damage is observed in the $Al_{0.9}Ga_{0.1}As$ layer up to a dose of 5×10^{15} cm^{-2}; the dechanneling level [in Fig. 3(b)] has only increased slightly. When the irradiation dose reaches 8×10^{15} cm^{-2}, a damage peak is observed in the $Al_{0.9}Ga_{0.1}As$ layer, corresponding very closely in depth to the projected range R_p of the ions. Also, at the top interface, a narrow region of AlGaAs appears to be heavily damaged or even amorphized. Eventually, as the ion dose is increased further (1×10^{16} cm^{-2}, a continuous amorphous layer appears to form in the $Al_{0.9}Ga_{0.1}As$ layer; however, at this dose, crystallinity still remains within the $Al_{0.9}Ga_{0.1}As$ layer at the lower interface. This may be a result of lower energy deposition density and more efficient dynamic annealing in $Al_{0.9}Ga_{0.1}As$ toward the tail of the ion distribution, as is discussed later.

To gain more insight into the microscopic nature of the defects in the above structure, XTEM was employed on the sample implanted to a dose of 8×10^{15} cm^{-2}. The basic structure of the unimplanted sample is shown in Fig. 4(a) and the implanted sample is shown in Fig. 4(b), with both micrographs at the same magnification. The thicknesses of the top

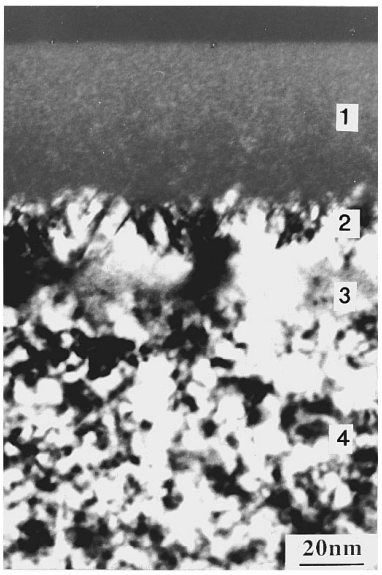

FIG. 5. Dark-field XTEM image of the same implanted sample as in Fig. 4(b) but at higher magnification, showing the high density of planar defects at the top interface within the $Al_{0.9}Ga_{0.1}As$ layer.

GaAs and underlying $Al_{0.9}Ga_{0.1}As$ layers are ~350 and ~1900 Å, respectively, The XTEM observations for the implanted sample are in excellent agreement with the channeling results and several distinct regions are clearly identifiable from Fig. 4(b). A continuous amorphous layer (region 1) is formed from the surface extending to a depth of ~520 Å. The thickness of this layer is larger than the initial GaAs layer, thereby confirming that the top interface has been amorphized and extends ~170 Å into the $Al_{0.9}Ga_{0.1}As$ layer. A band of planar defects (region 2) (100–200 Å thick) is seen immediately below this amorphous layer, followed by a region of relatively good crystal (region 3) (100–250 Å thick). The thick band of dark contrast (region 4) (900–1200 Å thick) indicates a heavily defected crystal corresponding closely in depth with the damage peak observed by RBS-C. The exact nature of the defect type in this region is difficult to identify but is most likely a result of defect clusters attributable to incomplete annihilation of irradiation-induced defects. Following this region is a layer of relatively good crystal (region 5) (250–500 Å thick). From comparison with the unimplanted sample, this crystalline region lies across the lower GaAs–$Al_{0.9}Ga_{0.1}As$ interface. A buried continuous amorphous layer (region 6) (~340 Å thick) appears in the underlying GaAs beyond this crystalline region. Below this layer is the good crystalline substrate (region 7). Figure 5 is the micrograph at higher magnification showing the microstructures of the top interface. The top amorphous–crystalline interface is decorated by many planar defects (region 2), which lie in the $Al_{0.9}Ga_{0.1}As$ layer.

It is interesting to note from XTEM results that there exists a narrow region in GaAs layers near the interface [region 5 in Fig. 4(b)] where adjacent $Al_{0.9}Ga_{0.1}As$ is able to inhibit ion-beam damage. The relatively good crystallinity of these regions suggest that dynamic annealing is dominant and amorphization is suppressed. One may argue that the high implantation dose gives rise to forward recoils and collisional mixing of these regions (i.e., increases the Al concentration in (GaAs) and, therefore, the onset of amorphization is delayed. However, as is shown later, the processes occurring at the interface are more complicated and the resultant interfacial disorder cannot be fully explained by direct ballistic intermixing. The residual damage is the result of a delicate balance among the various processes that occur at the interface. Another interesting point to note is that planar defects exist at the boundary between amorphous and crystalline AlGaAs. As discussed below, these may be formed during implantation as a result of the strong dynamic annealing in the AlGaAs layer or during a partial recrystallization process upon warming up to room temperature.

The above results from both MR439 and MR438 samples show that amorphization of the AlGaAs layer proceeds from the upper GaAs–AlGaAs interface. The AlGaAs layer with a higher Al content is not only more difficult to amorphize but is also able to offer more efficient protection against ion-beam damage to adjacent GaAs. In addition, in the case of the higher Al content structure, the higher concentration of implanted ions (due to higher implant doses used) may also act as trapping sites for mobile, irradiation-induced defects.

The damage buildup process in structures where the GaAs layer is sandwiched between two AlGaAs layers is illustrated in Fig. 6(b) for sample MR461 where a layer of GaAs sits in between two $Al_{0.9}Ga_{0.1}As$ layers. The peak in the atomic displacement distribution, from FASTRIM[25] calculations, now lies in the GaAs layer close to the top interface [Fig. 6(a)]. As expected, damage builds up preferentially in the GaAs layer. At the lowest dose of 6×10^{13} cm^{-2}, a buried amorphous layer is just about to form in the GaAs layer with very little damage observed in the top $Al_{0.9}Ga_{0.1}As$ layer. This buried amorphous layer then grows toward the interface and substrate with further bombardment. The determination of the interface position in these spectra is complicated. The depth scale plotted on the top axis is strictly valid only for the random spectrum. As shown in Fig. 6(b), good channeling is preserved in the overlaying $Al_{0.9}Ga_{0.1}As$ layer up to a dose of 5×10^{14} cm^{-2} (as a result of the low level of residual damage). Hence, due to the lower stopping power of channeled ions during analysis,[26] the depth scales of the aligned RBS-C spectra are actually compressed compared with the random spectrum. This results in the front edge of damage in GaAs appearing closer (in the RBS-C spectra) to the surface position than it actually is. As damage builds up in the overlaying $Al_{0.9}Ga_{0.1}As$, the effect of channeled ions is reduced (as a result of more scattering and dechanneling from defects) and the depth scale approaches that of the random spectrum. This effect is clearly seen in the spectrum for the sample irradiated to a dose of 5×10^{15} cm^{-2}. Hence, for the lower doses ($<5\times10^{15}$ cm^{-2}), there is a region of crystalline GaAs close to the upper GaAs–AlGaAs interface. This effect is quite interesting in the sense that it is inconsistent with the FASTRIM[25] calculation in which maximum energy deposition and, hence, amorphization is expected to proceed in the GaAs layer from the top interface. Eventually, as the dose is increased further, the crystalline interface region becomes unstable and amorphizes, allowing an amorphous phase to

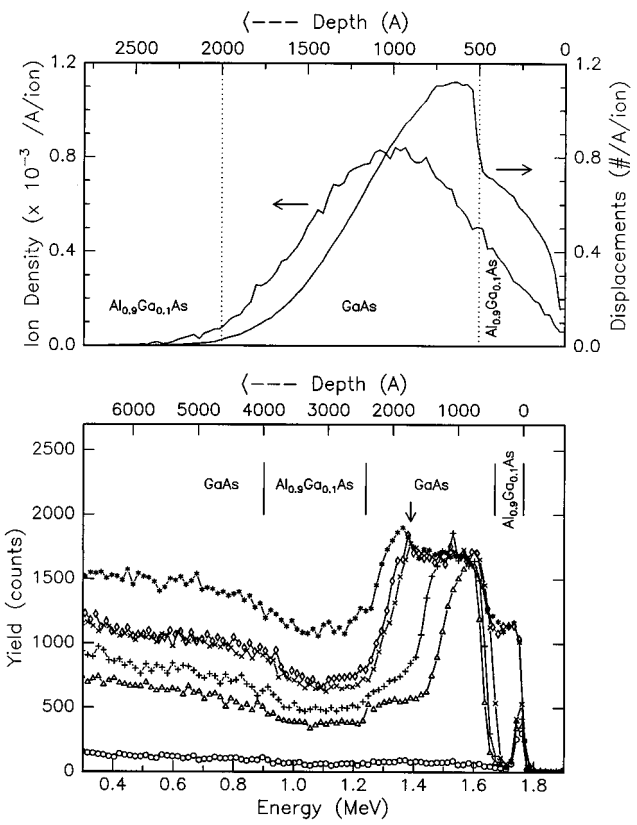

FIG. 6. RBS-C spectra (lower panel) showing the damage buildup for 90 keV Si^- irradiation of $Al_{0.9}Ga_{0.1}As/GaAs.Al_{0.9}Ga_{0.1}As/GaAs$ multilayer (MR461) at liquid-nitrogen temperature for various doses: unimplanted (○); 6×10^{13} cm^{-2} (△); 1×10^{14} cm^{-2} (+); 5×10^{14} cm^{-2} (×); 5×10^{15} cm^{-2} (◇); and random spectrum (*). The arrow indicates surface Al peak. Also shown in the upper panel is the displacement density profile as calculated by FASTRIM (Ref. 25).

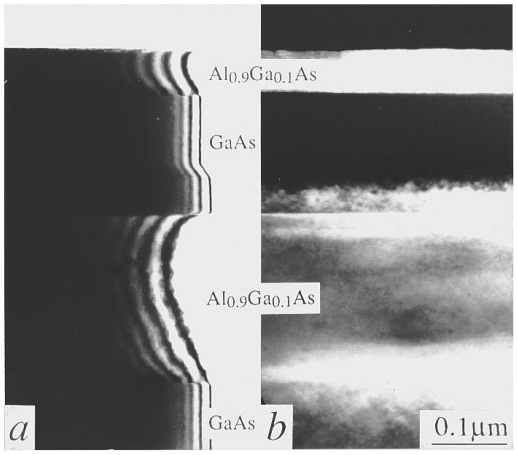

FIG. 7. (a) Bright-field XTEM image of a cleavage specimen from an unimplanted sample as in Fig. 6 (MR461) showing the basic structure, and (b) 400 dark-field ⟨110⟩ XTEM image of the same sample implanted to a dose of a 5×10^{15} cm^{-2}. Both images have the same magnification.

proceed into the overlaying $Al_{0.9}Ga_{0.1}As$, as shown for the dose of 5×10^{15} cm^{-2}. The underlying $Al_{0.9}Ga_{0.1}As$ has only a low level of crystalline defects due to the low-energy deposition density in this region and the efficiency of dynamic annealing of irradiation-induced point defects in $Al_{0.9}Ga_{0.1}As$. Note that the Al surface peak (arrowed) lies close to the lower GaAs–AlGaAs interface but even in the random spectrum, only contributes ~10% to the yield. In the corresponding channeled spectra, the effect is smaller and negligible.

An XTEM micrograph for the sample implanted to a dose of 5×10^{15} cm^{-2} is shown in Fig. 7(b), together with the unimplanted material in Fig. 7(a) for comparison. A buried amorphous layer is formed in the underlying GaAs layer with a tailing band of heavily defected material. No damage is observable in the underlying $Al_{0.9}Ga_{0.1}As$ layer while the top $Al_{0.9}Ga_{0.1}As$ layer retains its good crystallinity even though this region suffers a high degree of collisional displacements. The amorphous layer extends up to the top GaAs–$Al_{0.9}Ga_{0.1}As$ interface. This observation is consistent with the channeling effect (depth scale compression) during analysis of RBS-C spectra for doses $\leqslant5\times10^{15}$ cm^{-2}. Therefore, as observed by ion channeling, for doses less than 5×10^{15} cm^{-2}, there exist narrow regions in the GaAs layer, close to the GaAs–AlGaAs interface, in which amorphization is suppressed.

With AlGaAs of lower Al content, the degree of protection against ion-beam damage offered to the adjacent GaAs is lowered and dynamic annealing processes in AlGaAs during implantation become less efficient. This is illustrated by the RBS-C spectra in Fig. 8 for sample MR463 (GaAs sandwiched between two $Al_{0.5}Ga_{0.5}As$ layers). At 6×10^{13} cm^{-2}, very little damage is formed in GaAs adjacent to the top interface although a buried amorphous layer is formed within the GaAs layer (taking into account the channeling effect mentioned previously). With a small increase in dose to 1×10^{14} cm^{-2}, amorphization of this region occurs and proceeds very rapidly up to the GaAs–$Al_{0.5}Ga_{0.5}As$ interface. At

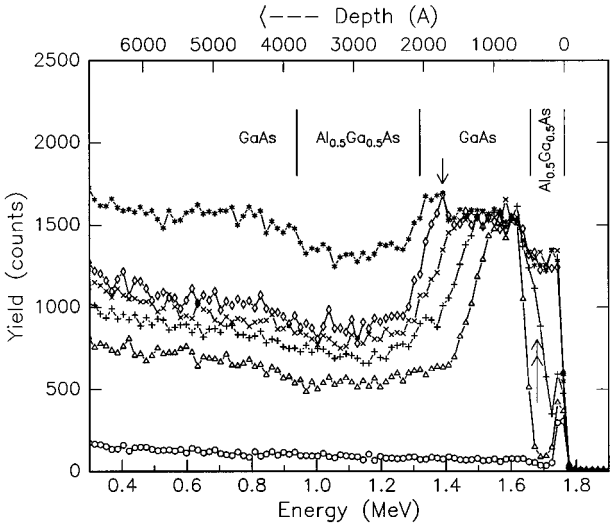

FIG. 8. RBS-C spectra showing the damage buildup for 90 keV Si^- irradiation of $Al_{0.5}Ga_{0.5}As/GaAs/Al_{0.5}Ga_{0.5}As/GaAs$ multilayer (MR463) at liquid-nitrogen temperature at various doses: unimplanted (○); 6×10^{13} cm^{-2} (△); 1×10^{14} cm^{-2} (+); 2×10^{14} cm^{-2} (×) 5×10^{14} cm^{-2} (◇); and random spectrum (*). The arrow indicates surface Al peak while the double-headed arrow indicates the damage peak in the overlaying $Al_{0.5}Ga_{0.5}As$.

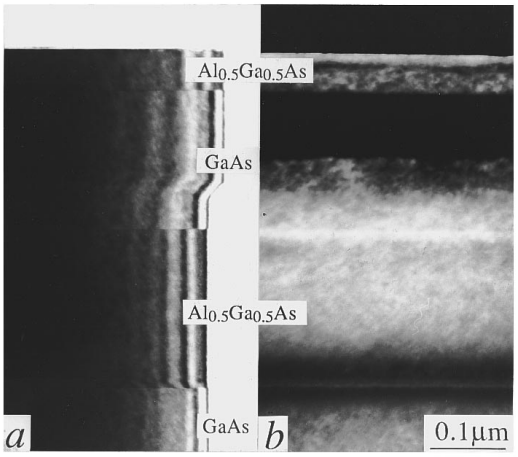

FIG. 9. (a) Bright-field XTEM image of a cleavage specimen from an unimplanted sample as in Fig. 8 (MR463) showing the basic structure, and (b) 400 dark-field ⟨110⟩ XTEM image of the same sample implanted to a dose of 1×10^{14} cm^{-2}. Both images have identical scale.

this instance a damage peak is also noted in the upper $Al_{0.5}Ga_{0.5}As$ layer (indicated by the double-headed arrow). This is in contrast with the previous results for $Al_{0.9}Ga_{0.1}As$, where, up to a dose of 5×10^{14} cm^{-2}, the interfacial dynamic annealing effect is still present and the $Al_{0.9}Ga_{0.1}As$ layer remains damage free. XTEM results for the implant at a dose of 1×10^{14} cm^{-2}, shown in Fig. 9, indicate that a buried amorphous layer of ~860 Å thick is formed in the GaAs layer, corresponding well with the RBS-C results. The top boundary of this amorphous layer extends up to the GaAs–$Al_{0.5}Ga_{0.5}As$ interface while the lower boundary extends into a band of heavily defected GaAs. Some damage contrast, most likely due to defect clusters, is observable in the top $Al_{0.5}Ga_{0.5}As$ layer at a depth which corresponds to the damage peak as observed by RBS-C. No defects are observable by XTEM at the lower GaAs–$Al_{0.5}Ga_{0.5}As$ interface, presumably due to the low displacement density and hence a dominant dynamic annealing effect at this interface.

Results shown thus far are for keV beams, where the displacement density or the rate of nuclear energy deposition is varying sharply across a narrow depth. To gain further insight into the interfacial effects, 1 MeV Si beams were used. At this energy the displacement density varies slowly across the region of interest, changing by less than a factor of 2 over the interfaces. The RBS-C results for MR463 (GaAs between two $Al_{0.5}Ga_{0.5}As$ layers) are shown in Fig. 10 together with the displacement density from FASTRIM[25] calculations. The maximum collisional displacement occurs at ~8500 Å from the surface, which is well below the layers of interest. The displacement density at the top GaAs layer is reduced approximately by a factor of 3–4 from the 90 keV case. Thus, at 1×10^{14} cm^{-2}, observable damage starts building up in underlying GaAs substrate, with only a small accumulation of damage in the upper GaAs layer. It should be noted that the depth scale is compressed as a result of channeling analysis—the front and back interfaces of the GaAs layer are indicated by double-headed arrows. The XTEM results in Fig. 11(a) indicate that a heavily defective band of material is formed in the GaAs substrate at a depth of ~8500

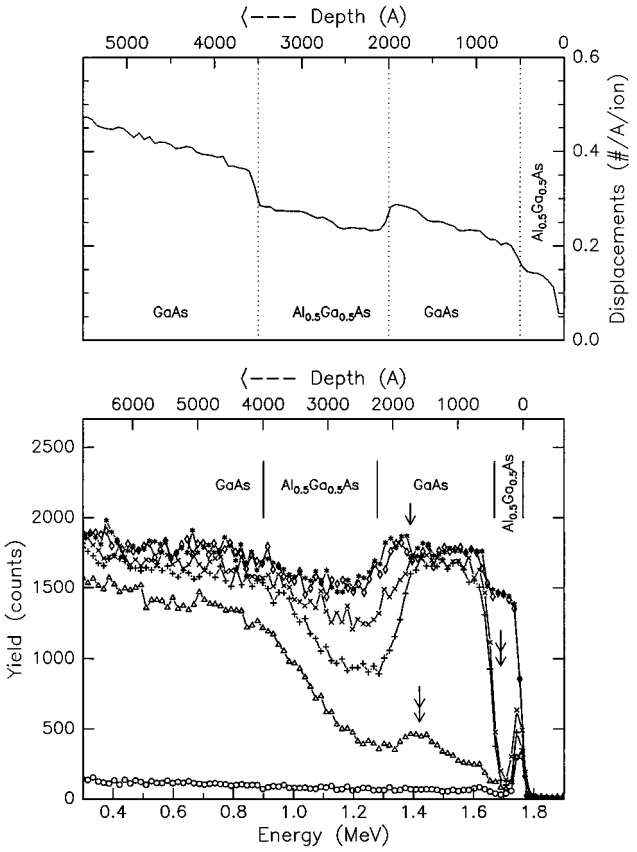

FIG. 10. RBS-C spectra (lower panel) showing the damage buildup for 1 MeV Si^+ irradiation of $Al_{0.5}Ga_{0.5}As/GaAs/Al_{0.5}Ga_{0.5}As/GaAs$ multilayer (MR463) at liquid-nitrogen temperature for various doses: unimplanted (○); 1×10^{14} cm^{-2} (△); 3×10^{14} cm^{-2} (+); 8×10^{14} cm^{-2} (×); 3×10^{15} cm^{-2} (◇); and random spectrum (*). The arrow indicates surface Al peak while the double-headed arrows indicate the front and back interface positions in the channel spectrum corresponding to the 1×10^{14} cm^{-2} case. Also shown in the upper panel is the displacement density profile as calculated by FASTRIM (Ref. 25).

Å, in excellent agreement with the FASTRIM[25] calculation of maximum collisional displacement depth. Careful analysis indicates that this defective band consists of planar faults co-existing with damage clusters. It is possible that amorphous zones within defective crystalline material are formed during irradiation and some recrystallization, as indicated by the presence of planar faults, has taken place during warm-up to room temperature. This observation is consistent with previous reports that incompletely amorphous GaAs recrystallizes upon warm-up to room temperature, leaving the characteristic signature of stacking faults.[27] The density of this damage decreases both toward the $Al_{0.5}Ga_{0.5}As$ layer and further into the substrate. From channeling results it can be noted that the level of damage in the upper GaAs layer appears to be slightly higher at the deeper interface (deeper arrow) than at the top interface (after a linear subtraction of the dechanneling level). The effect of the surface Al peak (arrowed), which one might expect to give rise to an apparent higher yield at the interface, is almost negligible in this case since, even in the random spectrum, the contribution from the Al signal is only ~5% of the total yield for $Al_{0.5}Ga_{0.5}As$. The slight asymmetrical effect at the interfaces

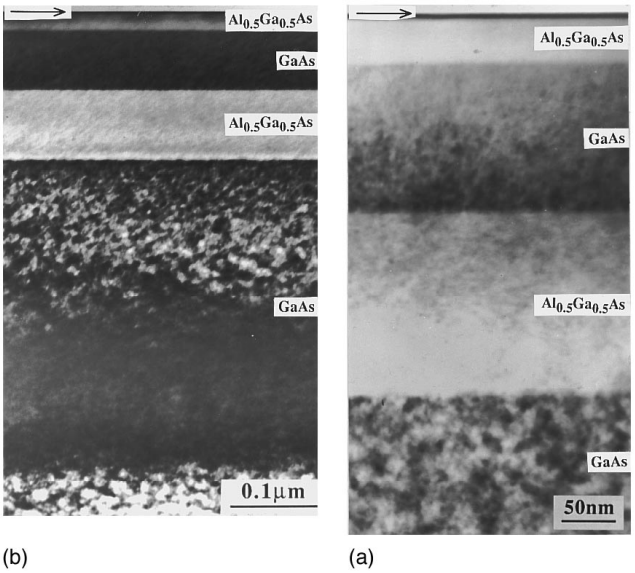

FIG. 11. (a) Bright-field XTEM image of the same sample as in Fig. 10 (MR463) implanted to a dose of 1×10^{14} cm^{-2} and (b) bright-field XTEM image of the same specimen at higher magnification, showing more details at the interfaces.

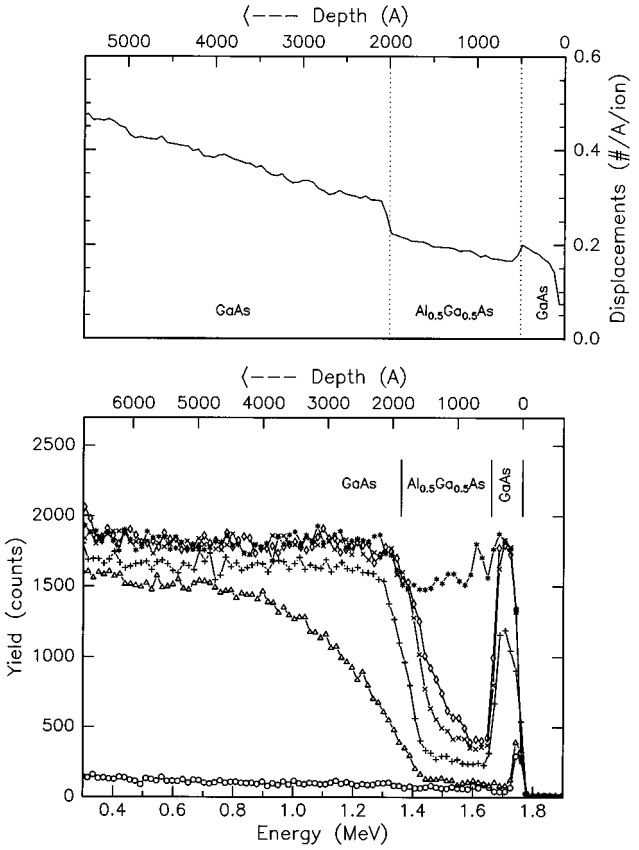

FIG. 12. RBS-C spectra (lower panel) showing the damage buildup for 1 MeV Si^+ irradiation of GaAs/$Al_{0.5}Ga_{0.5}As$/GaAs multilayer (MR439) at liquid-nitrogen temperature for various doses: unimplanted (○); 1×10^{14} cm^{-2} (△); 3×10^{14} cm^{-2} (+) 6×10^{14} cm^{-2} (×); 1×10^{15} cm^{-2} (◇); and random spectrum (*). Also shown in the upper panel is the displacement density profile as calculated by FASTRIM (Ref. 25).

(observed by RBS-C) is confirmed by the higher-magnification XTEM in Fig. 11(b), where the lower interface has a slightly stronger damage contrast than the upper interface. According to FASTRIM[25] calculations, the difference in displacement densities between the two interfaces is about 40% [Fig. 10(a)]. It is, therefore, not unreasonable to attribute the difference in residual damage densities at both interfaces to the difference in displacement densities; however, it is important to note that the residual damage after strong dynamic annealing is considerably less than that arising directly from displacement damage. At the higher dose of 3×10^{14} cm^{-2}, RBS-C indicates that a heavily damaged, possibly continuously amorphous, layer has formed in the top GaAs layer. This dose, at 1 MeV, is in reasonable agreement with the threshold dose for amorphization of GaAs with 90 keV beams after scaling it by the ratio of displacement densities for the two energies. Eventually, as the dose is increased further, complete amorphization of the top GaAs layer occurs and the amorphous–crystalline interface rapidly extends into the underlaying and overlaying $Al_{0.5}Ga_{0.5}As$ layers. Residual damage appears to accumulate faster in the deeper $Al_{0.5}Ga_{0.5}As$ layer than at the near-surface one (which can clearly be distinguished from the channeling spectrum at a dose of 8×10^{14} cm^{-2}) and this again can be attributed to the small difference in displacement densities between the top and bottom $Al_{0.5}Ga_{0.5}As$ layers [Fig. 10(a)].

Further results indicating the slight asymmetry of damage accumulation at the various interfaces are shown in Fig. 12 from RBS-C analysis. In this case, sample MR439 ($Al_{0.5}Ga_{0.5}As$ in between two GaAs layers) was irradiated by a 1 MeV Si^+ beam. Figure 12 shows that, at the lowest dose (1×10^{14} cm^{-2}), damage builds up in the substrate with the overlaying GaAs and $Al_{0.5}Ga_{0.5}As$ layers remaining fairly defect free. At the next highest dose of 3×10^{14} cm^{-2}, damage builds up asymmetrically across the top GaAs layer, being slightly higher at the back edge. Also, the ability of $Al_{0.5}Ga_{0.5}As$ to offer protection against ion-beam damage to adjacent GaAs regions is clearly observed at the upper and lower GaAs–$Al_{0.5}Ga_{0.5}As$ interfaces (taking into account of the channeling effect during analysis). A further increase in the dose to 6×10^{14} cm^{-2} results in the collapse of the near-interfacial GaAs regions to an amorphous phase and also the amorphization of the top GaAs layer. At the dose of 1×10^{15} cm^{-2}, amorphization has extended up to the lower GaAs–$Al_{0.5}Ga_{0.5}As$ interface and damage starts to nucleate into the $Al_{0.5}Ga_{0.5}As$ layer from the lower GaAs–$Al_{0.5}Ga_{0.5}As$ interface, consistent with the somewhat higher displacement density at the lower interface. Note that the slight increase in dechanneling level in the $Al_{0.5}Ga_{0.5}As$ layer for doses $\leqslant 6\times10^{14}$ cm^{-2} is consistent with little damage in this layer.

To further investigate the correlation between the asymmetrical disordering effect and the displacement density, 4 MeV Si^+ bombardment was carried out. The results are shown in Figs. 13(a) and 13(b) for samples MR463 and MR461, respectively, At this energy, the displacement density across the buried GaAs layer is almost constant (to within 10%). Although the channeling yield at the back interface is slightly higher than that at the top interface, this

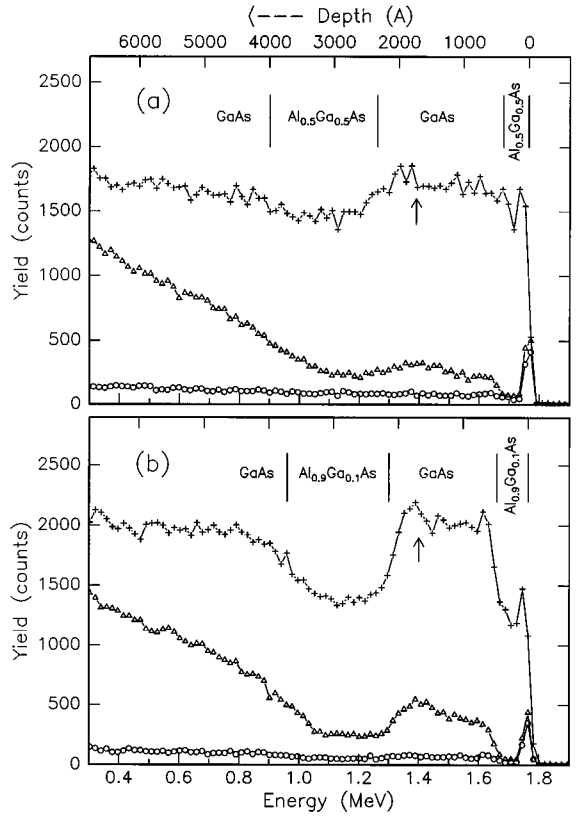

FIG. 13. RBS-C spectra of (a) $Al_{0.5}Ga_{0.5}As/GaAs/Al_{0.5}Ga_{0.5}As/GaAs$ multilayer (MR463), and (b) $Al_{0.9}Ga_{0.1}As/GaAs/Al_{0.9}Ga_{0.1}As/GaAs$ multilayer (MR461) irradiated with 4 MeV Si^+ at liquid-nitrogen temperature at a dose of 4×10^{14} cm^{-2} (△). The unimplanted sample (○) and the random spectrum (+) are as labeled. Arrows indicate surface Al peak.

effect is consistent with dechanneling of ions as they traverse a region of uniform (low-level) damage. The presence of uniform damage in the GaAs layer is confirmed after a linear subtraction of the dechanneling yield, taking into account of the small Al surface peak (arrowed).

DISCUSSION

The damage buildup and dynamic annealing processes in the GaAs–AlGaAs multilayer system are substantially more complex than the behavior observed in bulk GaAs or AlGaAs.[11,23] Damage accumulation occurs preferentially in the GaAs layer. This is not surprising as it has previously been reported that AlGaAs is increasingly more resistant to ion-beam damage with increasing Al content.[11–16,23] This trend is consistently observed in all GaAs–AlGaAs multilayer structures in this study. However, the strong dynamic annealing effects close to GaAs–AlGaAs interfaces at low implantation doses and preferential amorphization of AlGaAs at the interfaces at higher doses are further complexities observed in our studies. It is well known[23,28] that damage and amorphization processes created by medium to heavy mass ions in bulk GaAs at LN2 temperatures can be best described by a heterogeneous amorphization model.[29] In this model, the disorder consists of localized damage clusters and even small pockets of amorphous material created by individual ions. Very little dynamic annealing takes place at such implantation temperatures where irradiation-induced defects are ''frozen in.'' A continuous amorphous layer is eventually formed via the overlap of these defective zones. Damage and amorphization processes in thick (bulk) AlGaAs layers, on the other hand, are more complex.[23] At low and moderate Al compositions, the damage buildup process seems best modeled by a heterogeneous process, but with some dynamic annealing of the implantation disorder taking place even at LN2 temperatures. Hence, the residual damage in AlGaAs is a result of the competition between dynamic annealing and damage production by the incoming ions (i.e., the nuclear energy deposition density). Dynamic annealing also becomes more efficient with increasing Al content.[23] At high Al content, however, the damage and amorphization processes appear to be best described by a homogeneous model,[30,31] in which disorder is accumulated (in the form of crystalline defect clusters in our case)[12,23] until a critical defect level is reached (corresponding to a critical free energy of the defective system), after which the structure collapses into a lower-free-energy, amorphous phase. The dynamic annealing in AlGaAs is most likely a result of the mobility of point defects (vacancies and/or interstitials) as discussed previously.[23] Since no dependency of the residual damage on the dose rate was observed in AlGaAs at LN2 in our previous study,[23] the time scale in which dynamic annealing occurs is fast compared with the time between overlap of individual damage cascades, at least under our irradiation conditions. Indeed, it is unlikely that strong dynamic annealing in AlGaAs can occur without at least short-range mobility of such defects.

In multilayer structures the nature of damage accumulation in a GaAs layer is more complex than in bulk (thick) material. The heterogeneous model appears to be only applicable for GaAs regions away from GaAs–AlGaAs interfaces. At these interfaces, dynamic annealing inhibits complete amorphization at the lower doses even at LN2 temperatures. Therefore, consistent with previous studies,[11–22] the presence of AlGaAs offers some protection against damage accumulation in adjacent GaAs regions. This is the case even when the maximum in collisional displacements occurs at the interface. It has been proposed[16] that intermixing effects increase the Al content in GaAs layers adjacent to AlGaAs and thus increase their resistance to ion-beam damage. Our results do not support an intermixing model since at lower doses ($<1\times10^{15}$ cm^{-2}), where ballistic intermixing is expected to be negligible, the interfacial effect is still quite pronounced. In addition, at higher doses where intermixing is expected to increase, we observe interfacial amorphization rather than dynamic annealing. Intermixing as a result of thermal diffusion is also expected to be small since the diffusion coefficients of Ga and Al in GaAs–AlGaAs multilayers are very small[32,33] and no thermal treatment occurred besides warming up to room temperature. Another suggestion by Cullis *et al.*[17,18] to explain the interfacial dynamic annealing effect is that AlGaAs (AlAs) layers act as a local sink for mobile point defects induced during irradiation in these narrow GaAs regions, resulting in suppression of defect accumulation in GaAs and, hence, inhibition of amorphization. Restructuring of the GaAs may also be en-

hanced by point-defect interaction and annihilation, involving, for example, Al-related defect species. However, this proposal does not satisfactorily explain some of our observations, in particular, the final amorphization of these regions at higher doses.

In view of both our detailed observations and the above arguments, we suggest the following phenomenological model. First, we summarize the observations and implications for damage accumulation in both GaAs and AlGaAs layers as a result of the impinging Si ions. At low doses, ion-generated defects are stable in the GaAs layers, but, due to the strong dynamic annealing in AlGaAs (as a result of defect mobility and/or local bonding rearrangements),[11] very little residual damage remains in these layers. Also, at low doses the small incorporation of Si ions within the lattice (<0.1 at. %) should not present any observable increased nucleation effect for defect clustering or amorphization. A further increase in the ion dose creates an amorphous phase in GaAs layers by a heterogeneous process except for narrow regions of defective crystal near the GaAs–AlGaAs interfaces; however, the remaining defective crystalline regions at the interfaces collapse into an amorphous phase above a critical defect density at higher irradiation doses. Once an amorphous phase is formed in these regions, amorphization proceeds rapidly layer by layer into the adjacent AlGaAs layers. Also, at high doses the high concentration of Si ions (often exceeding 1 at. %) at R_p is also a potential environment for eventual stabilization of defects and nucleation of amorphous zones in AlGaAs, despite the strong dynamic annealing in this alloy; however, interfaces appear to be preferred sites for nucleating amorphous material.

It is instructive to explore possible mechanisms to account for the above observations. We suggest that the suppression of amorphization in GaAs close to AlGaAs layers arises from mobile point defects generated in AlGaAs. Indeed, the dynamic annealing of AlGaAs arises from local bonding rearrangement and/or point-defect mobility in this material even at LN2 temperatures during irradiation;[23] however, the dynamic annealing does not result in complete annihilation of defects and the residual damage in AlGaAs consists of dilute point-defect clusters or extended defects. We propose that some of the point defects generated in AlGaAs during irradiation are injected across the interface into adjacent GaAs regions. The mechanism of such defect injection cannot be conclusively proven from this experiment but it is likely to be a result of point-defect diffusion. This is consistent with the likely presence of mobile point defects in AlGaAs, as a result of the observed strong dynamic annealing. At low doses, we suggest that the diffusion of these mobile defects mediates *in situ* annealing of the GaAs lattice close to the interface, thereby inhibiting complete amorphization; however, the *in situ* annealing is not perfect and the residual crystalline defects at the interface result in an increase of the system's free energy. Also, as the density of crystalline defects increases, the effectiveness of dynamic annealing in this region may be reduced. Eventually, amorphization is achieved at higher doses when the free energy exceeds a critical limit. At this stage, the crystalline regions relax into an amorphous phase, thereby lowering the local free energy by relieving strain energy. This is not unlike damage accumulation and amorphization in high-Al-content AlGaAs that has previously been reported[23] and which is best described by a homogeneous amorphization process.[30,31] Once amorphization of these interface regions has eventually occurred, point defects injected from the AlGaAs layers may then agglomerate at the amorphous–crystalline boundary rather than annihilate. The amorphous–crystalline interface may then become a nucleating site for amorphization which extends (layer by layer) across the interface into the AlGaAs layer. This effect has also been observed in Si under certain irradiation conditions.[12] Hence, GaAs–AlGaAs interface regions behave not only as a supply of point defects to facilitate dynamic annealing (below a critical dose) but also as a sink for point defects and a nucleating site for amorphization of AlGaAs once an amorphous layer has formed up to the interface (above a critical dose). In alloys with higher Al content, defect mobility and *in situ* annealing across the interface become more efficient and higher doses are required to nucleate amorphous layers.

It is further interesting to explore the dependence of damage buildup on energy deposition density. The damage buildup in GaAs is dependent on the nuclear energy deposition density (i.e., atomic displacements), the maximum damage corresponding to the maximum in the energy deposition distribution; however, the damage buildup in AlGaAs is a result of the competition between dynamic annealing and nuclear energy deposition density. The nuclear energy deposition density varies with depth along the damage cascade. Toward the tail of each cascade, where energy deposition and hence the damage production rate is low, dynamic annealing may dominate. The resulting residual damage in these regions could be very different from other parts of the sample near the peak of the distribution where the number of displaced atoms is much higher. Indeed, we do observe differences in residual disorder throughout the AlGaAs layers, where the changes are consistent with differences in the energy deposition distribution of keV ions. We also note that, for amorphization of AlGaAs layers, the buildup of damage is not only dependent on local energy deposition density but also strongly influenced by annealing and/or defect trapping processes occurring at GaAs–AlGaAs interfaces, as discussed earlier.

With MeV beams, the nuclear energy deposition density is much reduced in the near-surface region and amorphization would be expected to occur at proportionately higher doses, as is observed for both GaAs and AlGaAs layers. However, since MeV beams penetrate entirely through the layers with slowly varying energy deposition density with depth, it is interesting to compare the damage and dynamic annealing processes at the top and bottom GaAs–AlGaAs interfaces. With 1 MeV beams, a slight asymmetry in the residual damage is observed between the interfaces; with damage first building up at the deeper interface. This effect has been reported previously[20–22] and Klatt *et al.*[20] related it to the ratio of the electronic (ionization) to nuclear (damage) energy loss of the incoming ions; however, our results from MeV implants do not support this explanation. For 4 MeV irradiation, despite a 30%–40% difference in the ratio of

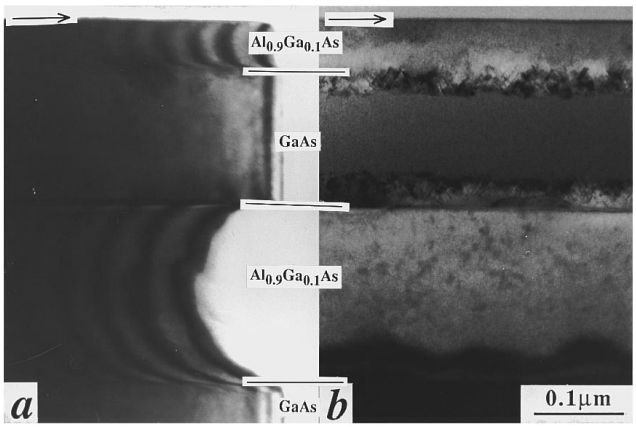

FIG. 14. (a) Bright-field XTEM image of a cleavage specimen from an unimplanted sample as in Fig. 7 (MR461) showing the basic structure, and (b) bright-field XTEM image of the same sample implanted to a dose of a 5×10^{15} cm^{-2}. Both images have the same magnification. The implanted sample has been subjected to 160 °C heating during specimen preparation. Note the two bands of planar defects at the amorphous–crystalline interfaces.

electronic to nuclear energy losses across the interfaces, damage accumulation is relatively constant throughout the layer, consistent with the relatively constant displacement density. Furthermore, for 1 MeV irradiation, where the displacement density varies by ~40% across the interfaces, a higher degree of asymmetry in the residual damage density is observed. In our case, it is difficult to ascertain whether the increase in residual disorder at the deeper interface is consistent with increased energy deposition or whether some other cause is appropriate. For example, Turkot *et al,*[22] also observed increased damage at a deeper AlGaAs–GaAs interface but suggested that the amount of damage could not be accounted for by increased energy deposition alone. They proposed that energetic recoil events in a particular energy range cause a larger number of cascades and intermixing at the deeper interface thus explaining the increased disorder. We cannot determine from our data whether this might also be occurring in our case; however, we note again that there is strong dynamic annealing at such interfaces and correlations of ''amounts'' of residual disorder directly with nuclear energy deposition processes is fraught with difficulty.

In some cases in our studies the exact nature of the residual damage following implantation at LN2 temperatures is not clearly known. The observed residual disorder appears to be dependent on the (thermal) stability of defects in these regions generated during LN2 irradiation and following subsequent heating such as warming up to room temperature and during XTEM specimen preparation. As an illustration, the micrograph in Fig. 14 is the same specimen as that in Fig. 7 but has been subjected to 160 °C epoxy curing during XTEM sample preparation. An instability of interface disorder is confirmed by the observed planar defects in the GaAs layer at the amorphous–crystalline interfaces, indicating partial recrystallization of the amorphous GaAs layer has taken place. This effect is quite surprising in this multilayer system because recrystallization of an amorphous GaAs layer occurs at a much lower temperature than normally observed in bulk GaAs.[34–36]. This type of recrystallization, which does not occur in bulk GaAs, is efficient in GaAs regions close to adjacent AlGaAs layers which may provide a ready source of point defects with increased mobility during low-temperature heating. In AlGaAs, however, the interfacial instability is more pronounced (Figs. 4 and 5) as indicated by the presence of planar defects (region 2) at the amorphous–crystalline interface. It is possible that, once an amorphous phase is formed in AlGaAs, the amorphous regions act as trapping sites for point defects and, due to strong local bonding rearrangements, planar defects are formed (so as to lower the system's free energy) during irradiation. However, it is equally likely that the residual damage following implantation consists of overlapping defect clusters or amorphous pockets in such cases. Upon warming the sample up to room temperature, these partly amorphous regions recrystallize imperfectly in the presence of surrounding crystalline material (which acts as the seed for recrystallization) into planar defects. The instability of incomplete amorphous material in AlGaAs during warm up to room temperature has previously been observed in bulk AlGaAs layers[23] and also in multilayers;[22] however, no comprehensive explanation of such low-temperature annealing effects has been put forward. Despite the possibility of some annealing (on warm-up to room temperature) of incomplete amorphous regions in AlGaAs, there is little evidence from our previous study[23] or in the present work to suggest recovery of complete amorphous regions in high-Al-content AlGaAs.

CONCLUSIONS

We have systematically studied the damage buildup and amorphization processes of GaAs–AlGaAs multilayers at LN2 temperatures. These processes are more complex than those in bulk GaAs or AlGaAs. Damage builds up preferentially in the GaAs layer but the presence of adjacent AlGaAs layers inhibit disorder formation in narrow regions of GaAs close to the interface. This effect is accentuated with increasing Al content. Dynamic annealing, as mediated by defect trapping and defect migration, competes very strongly with damage production at the interface and residual damage is the result of a fine balance between these two processes. Once amorphous layers eventually form at GaAs–AlGaAs interfaces at sufficiently high implantation doses, they act as nucleation sites for the progression of the amorphous phase into the AlGaAs layers. The presence of adjacent AlGaAs also appears to enhance the recrystallization of amorphous GaAs at low temperature, presumably by lowering the recrystallization temperature through the supply of mobile defects.

ACKNOWLEDGMENTS

The authors would like to thank A. Clark and G. Li for their assistance in growing the structures and A. Sikorski and T. T. Ye for preparing the XTEM samples. H. H. T. acknowledges the financial assistance from AIDAB. J. Z. would like to thank the Australian Research Council for an Australian Postdoctoral Research Fellowship.

[1] W. D. Laidig, N. Holonyak, Jr., M. D. Camras, K. Hess, J. J. Coleman, P. D. Dupkus, and J. Bardeen, Appl. Phys. Lett. **38**, 776 (1981).
[2] J. J. Coleman, P. D. Dupkus, C. G. Kirkpatrick, M. D. Camras, and N. Holonyak, Jr., Appl. Phys. Lett. **40**, 904 (1982).
[3] F. E. Prins, G. Lehr, H. Schweizer, and G. W. Smith, Appl. Phys. Lett. **63**, 1402 (1993).
[4] T. Hirata, M. Maeda, M. Suehir, and H. Hosomatsu, Jpn. J. Appl. Phys. **29**, L961 (1990).
[5] J. Cibert, P. M. Petroff, G. J. Dolan, S. J. Pearton, and J. H. English, Appl. Phys. Lett. **49**, 1275 (1986).
[6] F. Xiong, T. A. Tombrello, H. Wang, T. R. Chen, H. Z. Chen, H. Morkoç, and A. Yariv, Appl. Phys. Lett. **54**, 730 (1989).
[7] T. Fukuzawa, S. Semura, H. Saito, T. Ohta, Y. Uchida, and H. Nakashima, Appl. Phys. Lett. **45**, 1 (1986).
[8] A. N. M. Mason Choudhury, P. Melman, A. Silletti, E. S. Koteles, B. Foley, and B. Elman, IEEE Photon. Technol. Lett. **PTL-3**, 817 (1991).
[9] S. J. Pearton, Mater. Sci. Rep. **4**, 313 (1990).
[10] S. J. Pearton, F. Ren, J. R. Lothian, T. R. Fullowan, A. Katz, P. W. Wisk, C. R. Abernathy, R. F. Kopf, R. G. Elliman, M. C. Ridgway, C. Jagadish, and J. S. Williams, J. Appl. Phys. **71**, 4949 (1992).
[11] J. S. Williams, C. Jagadish, A. Clark, G. Li, and C. A. Larsen, Nucl. Instrum. Methods B **74**, 80 (1993).
[12] J. S. Williams, H. H. Tan, R. D. Goldberg, R. A. Brown, and C. Jagadish, Mater. Res. Symp. Proc. **316**, 15 (1994).
[13] A. G. Cullis, A. Polman, P. W. Smith, D. C. Jacobson, J. M. Poate, and C. R. Whitehouse, Nucl. Instrum. Methods B **62**, 463 (1992).
[14] I. Jencic, M. W. Bench, and I. M. Robertson, J. Appl. Phys. **69**, 1287 (1991).
[15] I. Jencic, M. W. Bench, I. M. Robertson, M. A. Kirk, and J. Peternelj, Nucl. Instrum. Methods B **59/60**, 458 (1991).
[16] C. Vieu, M. Schneider, H. Launois, and B. Descouts, J. Appl. Phys. **71**, 4833 (1992).
[17] A. G. Cullis, N. G. Chew, C. R. Whitehouse, D. C. Jacobson, J. M. Poate, and S. J. Pearton, Appl. Phys. Lett. **55**, 1211 (1989).
[18] A. G. Cullis, P. W. Smith, D. C. Jacobson, and J. M. Poate, J. Appl. Phys. **69**, 1279 (1991).
[19] D. J. Eaglesham, J. M. Poate, D. C. Jacobson, M. Cerullo, L. N. Pfeiffer, and K. West, Appl. Phys. Lett. **58**, 523 (1991).
[20] J. L. Klatt, R. S. Averback, D. V. Forbes, and J. J. Coleman Phys. Rev. B **48**, 17 629 (1993).
[21] B. A. Turkot, I. M. Robertson, M. A. Kirk, L. E. Rehn, P. M. Baldo, D. V. Forbes, and J. J. Coleman, *Microstructure of Irradiated Materials*, edited by I. M. Robertson, S. J. Zinkle, L. E. Rehn, and W. J. Phythian (1995), p. 451.
[22] B. A. Turkot, D. V. Forbes, I. M. Robertson, J. J. Coleman, L. E. Rehn, M. A. Kirk, and P. M. Baldo, J. Appl. Phys. **78**, 97 (1995).
[23] H. H. Tan, C. Jagadish, J. S. Williams, J. Zou, D. J. H. Cockayne, and A. Sikorski, J. Appl. Phys. **77**, 87 (1995).
[24] J. F. Ziegler, J. P. Biersack, and U. Littmark, in *The Stopping and Range of Ions in Solid*, edited by J. F. Ziegler (Pergamon, New York, 1985).
[25] H. J. Hal, FASTRIM is a modified version of TRIM85-90 which takes into account of the multilayer target problems inherent with TRIM (unpublished).
[26] *Ion-Beam Analysis*, edited by J. R. Bird and J. S. Williams (Academic, Australia, 1989).
[27] J. S. Vetrano, M. W. Bench, I. M. Robertson, and M. A. Kirk, Metall. Trans. A **20**, 2673 (1989).
[28] D. K. Sadana, Nucl. Instrum. Methods B **7/8**, 375 (1985).
[29] F. Morehead and B. L. Crowder, Radiat. Eff. **6**, 27 (1970).
[30] F. L. Vook, *Radiation Damage and Defects in Semiconductors* (Institute of Physics, London, 1971), p. 60.
[31] M. L. Swanson, J. R. Parsons, and C. W. Hoelke, Radiat. Eff. **9**, 249 (1971).
[32] P. M. Petroff, J. Vac. Sci. Technol. **14**, 973 (1977).
[33] R. M. Fleming, D. B. McWhan, A. C. Gossard, W. Wiegmann, and R. A. Logan, J. Appl. Phys. **51**, 357 (1980).
[34] S. S. Kular, B. J. Sealy, K. G. Stephens, D. K. Sadana, and G. R. Booker, Solid-State Electron. **23**, 831 (1980).
[35] C. Licoppe, Y. I. Nissim, and P. Heroc, Appl. Phys. Lett. **48**, 1441 (1986).
[36] S. Yokoyama, D. Yui, H. Tanigawa, H. Takasugi, and M. Kawabe, J. Appl. Phys. **62**, 1808 (1987).